Supplementary Information

Comparison of Fast Electron Transfer Kinetics at Platinum, Gold, Glassy Carbon and Diamond Electrodes using Fourier-Transformed AC Voltammetry and Scanning Electrochemical Microscopy

Sze-yin Tan,[a,b] Robert A. Lazenby,[a,c] Kiran Bano,[b,d] Jie Zhang,[*,b] Alan M. Bond,[*,b] Julie V. Macpherson,[a] Patrick R. Unwin*[,a]

[a] Department of Chemistry, University of Warwick, Coventry, West Midlands CV4 7AL, United Kingdom

[b] School of Chemistry, Monash University, Clayton, Victoria 3800, Australia

[c] Present address: Department of Chemistry and Biochemistry, University of Maryland Baltimore County, Baltimore, Maryland 21250, United States

[d] Present address: School of Chemistry, University of Connecticut, Storrs, Connecticut 06269, United States

* To whom correspondence should be addressed. E-mail: jie.zhang@monash.edu, alan.bond@monash.edu and p.r.unwin@warwick.ac.uk

Contents

Section S1: Fourier-transformed large amplitude alternating current voltammetry (FTACV): theory and simulations

FTACV simulations were carried out with the MECSim program written in Fortran.[1,2] Fick's law of planar diffusion was solved numerically to determine the electrochemical response by applying Butler-Volmer[3,4] formulations to describe the potential-dependence of electron transfer (ET) at the electrode/electrolyte interface.

The direct current (DC) potential ramp applied to the working electrode was superimposed with an alternating current (AC) sine wave of amplitude, ΔE = 80 mV and frequency, f = 228.0 Hz. The FTACV data obtained experimentally and theoretically were converted from the time domain to the frequency domain using a Fourier-transform algorithm. Frequencies corresponding to the AC harmonic components were selected from the power spectrum and were subjected to band filtering and inverse Fourier-transform procedures to obtain the resolved AC components as a function of time. Electrode area, A, solution concentration, c, uncompensated resistance, R_u, and diffusion coefficients, D, are known from other measurements while the redox couple formal potential, $E^{0'}$, standard heterogeneous rate constant, k^0, transfer coefficient, α and the double layer capacitance, C_{dl} were computed in FTACV simulations. $E^{0'}$ can also be estimated from the potential minima and maxima of the even and odd harmonics, respectively. The potential-dependent C_{dl} was determined from the fundamental harmonic component in the potential region where there is no faradaic current and is modeled as a fourth-order polynomial function: $C_{dl} = c_0 + c_1E + c_2E^2 + c_3E^3 + c_4E^4$, where c_0, c_1, c_2, c_3 and c_4 are constants. R_u was determined from the 1st and 2nd AC harmonics. The higher order harmonic components (3rd to 7th), which are highly sensitive to electrode kinetics, were used to determine k^0. α is reasonably assumed to be 0.5.

The least squares correlation, Ψ, between experimental and simulated data is given by the following:[5,6]

$$\Psi = 1 - \left[\frac{1}{H} \left(\sum_{h=1}^{H} \sqrt{\frac{\sum_{i=1}^{N} \left[(f_h^{\exp}(x_i) - f_h^{sim}(x_i))^2 \right]}{\sum_{i=1}^{N} f_h^{\exp}(x_i)^2}} \right) \right] \quad \text{(eqn S1)}$$

where h is the number of the AC harmonic component, H is the total number of AC harmonic components considered and $f_h^{\exp}(x_i)$ and $f_h^{\text{sim}}(x_i)$ are the experimental and simulated functions in the corresponding AC harmonic, respectively and N is the number of data points. All calculations of Ψ do not include the first and last 0.5 s of the FTACV scan to ensure effects of 'ringing' artefacts resulting from the experimental Fourier-transform – band filtering – inverse Fourier-transform process do not reduce the reliability of the simulated fit and is described in detail elsewhere.[7]

Section S2: Scanning electrochemical microscopy (SECM): tip positioning

A scanning electrochemical microscope (SECM) was mounted on a vibration-isolation table inside a Faraday cage. The ultramicroelectrode (UME) tip (radius, a = 1 μm and insulating glass/active electrode radius ratio, RG = 20) was mounted in a tip holder on a piezo-bender actuator, to which an oscillation (70 Hz with an amplitude of 50 nm (~ 5 % UME tip electrode radius)) was applied. In turn, this was mounted on a 3D-piezoelectric positioner controlled by a PC running custom LabVIEW code (LabVIEW 9.0, National Instruments), which was also used for data acquisition. The tip-substrate separation was controlled by monitoring the damping of the oscillation amplitude of the tip upon intermittent-contact between the tip and surface (typically by 5 %).[8]

Section S3: SECM: theory

Determination of mass transport parameters: positive feedback approach curve

The steady-state diffusion limited UME tip current in bulk solution, $i_{\mathrm{UME,bulk}} = 4nFaDc$, where n is the number of electrons transferred per redox event and F is the Faraday constant, was used to normalised UME tip currents measured close to the substrate electrode, at distance, d. The normalised tip-substrate separation, $L = d/a$, is reliably determined from normalised diffusion-limited positive feedback currents, $I_{\mathrm{UME,lim}}$:[9]

$$I_{\mathrm{UME,lim}}(L,\mathrm{RG}) = \alpha(\mathrm{RG}) + \frac{\pi}{4\beta(\mathrm{RG})\arctan(L)} + \left(1-\alpha(\mathrm{RG})-\frac{1}{2\beta(\mathrm{RG})}\right)\left(\frac{2}{\pi}\arctan(L)\right) \qquad \text{(eqn S2)}$$

with

$$\alpha(\mathrm{RG}) = \ln 2 + \ln 2\left(1-\frac{2}{\pi}\arccos\left(\frac{1}{\mathrm{RG}}\right)\right) - \ln 2\left(1-\left(\frac{2}{\pi}\arccos\left(\frac{1}{\mathrm{RG}}\right)\right)^2\right) \qquad \text{(eqn S3)}$$

and

$$\beta(\mathrm{RG}) = 1 + 0.639\left(1-\frac{2}{\pi}\arccos\left(\frac{1}{\mathrm{RG}}\right)\right) - 0.186\left(1-\left(\frac{2}{\pi}\arccos\left(\frac{1}{\mathrm{RG}}\right)\right)^2\right) \qquad \text{(eqn S4)}$$

Determination of kinetic and thermodynamic parameters: analytical model

Kinetic and thermodynamic properties for the redox processes in the substrate voltammetry SECM configuration are obtained by comparison of experimental curves to an analytical expression. The analytical expressions for the normalised tip current measured in both the competition and substrate generation/tip collection (SG/TC) modes for an oxidation process are given by the following:[10]

$$I_{\mathrm{comp,oxi}}(E_{\mathrm{sub}}, L) = \xi^2\left[\frac{\pi}{2\beta(\mathrm{RG})L(2\xi^2\theta_{\mathrm{sub}} + 2\theta_{\mathrm{sub}}{}^{\alpha}/\lambda^{o'} + \xi^2 + 1)} + \frac{1}{\xi\theta_{\mathrm{sub}} + 1}\left(\frac{I_{\mathrm{UME,lim}}(L)}{\xi^2} - \frac{\pi}{2\beta(\mathrm{RG})L(\xi^2+1)}\right)\right] \quad \text{(eqn S5)}$$

$$I_{\mathrm{sgtc,oxi}}(E_{\mathrm{sub}}, L) = -\xi^2\left[\frac{\pi}{2\beta(\mathrm{RG})L(2/\theta_{\mathrm{sub}} + 2\theta_{\mathrm{sub}}{}^{\alpha-1}/\lambda^{o'} + \xi^2 + 1)} + \frac{\xi\theta_{\mathrm{sub}}}{\xi\theta_{\mathrm{sub}} + 1}\left(\frac{I_{\mathrm{UME,lim}}(L)}{\xi} - \frac{\pi}{2\beta(\mathrm{RG})L(\xi^2+1)}\right)\right] \text{(eqn S6)}$$

with

$$\theta_{\mathrm{sub}} = \exp(F(E_{\mathrm{sub}} - E^{0'})/RT \quad \text{(eqn S7)}$$

and

$$\lambda^{0'} = k^{0'}d/D_{\mathrm{ox}} \quad \text{(eqn S8)}$$

and

$$\xi = \sqrt{\frac{D_{\mathrm{ox}}}{D_{\mathrm{red}}}} \quad \text{(eqn S9)}$$

where, ξ is the dimensionless diffusion coefficient ratio and $\lambda^{0'}$ is the dimensionless ET rate constant.

The analytical expressions for the normalised tip current vs substrate potential in competition and SG/TC modes for a reduction process are given by:[10]

$$I_{\text{comp,red}}(E_{\text{sub}}, L) =$$

$$-\left[\frac{\pi}{2\beta(\text{RG})L(2/\theta_{\text{sub}} + 2\theta_{\text{sub}}{}^{\alpha-1}/\lambda^{o'} + \xi^2 + 1)} + \frac{\xi\theta_{\text{sub}}}{\xi\theta_{\text{sub}} + 1}\left(I_{\text{UME,lim}}(L) - \frac{\pi}{2\beta(\text{RG})L(\xi^2 + 1)}\right)\right] \quad \text{(eqn S10)}$$

$$I_{\text{sgtc,red}}(E_{\text{sub}}, L) =$$

$$\frac{\pi}{2\beta(\text{RG})L(2\xi^2\theta_{\text{sub}} + 2\theta_{\text{sub}}{}^{\alpha}/\lambda^{o'} + \xi^2 + 1)} + \frac{1}{\xi\theta_{\text{sub}} + 1}\left(\frac{I_{\text{UME,lim}}(L)}{\xi} - \frac{\pi}{2\beta(\text{RG})L(\xi^2 + 1)}\right) \quad \text{(eqn S11)}$$

Section S4: Cyclic voltammetry (CV) at macrodisk electrodes for the oxidation of tetrathiafulvalene and reduction of tetracyanoquinodimethane

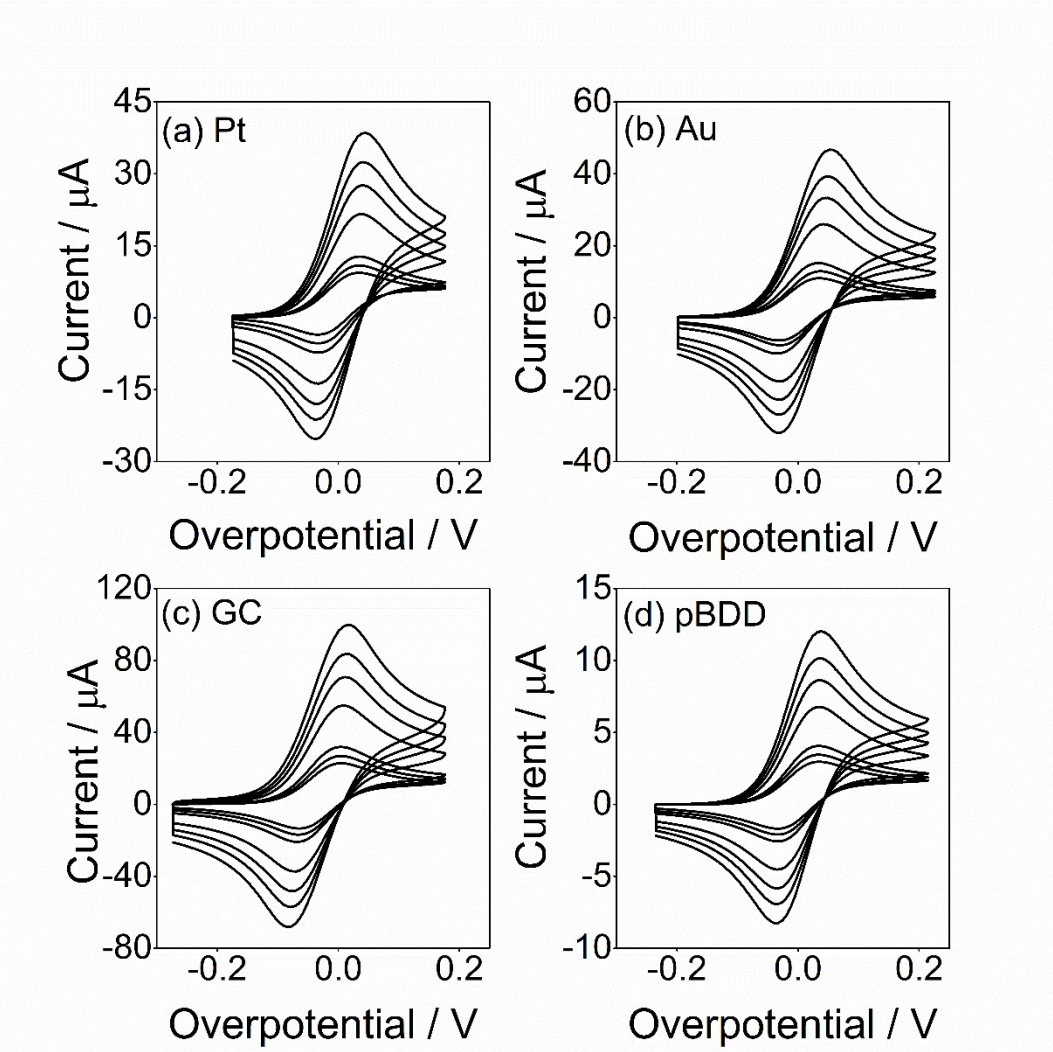

Figure S1. CVs for the oxidation of 1.0 mM TTF in CH_3CN (0.1 M Bu_4NPF_6) at (a) Pt (a_{Pt} = 1.0 mm), (b) Au (a_{Au} = 1.0 mm), (c) GC (a_{GC} = 1.5 mm) and (d) pBDD (a_{pBDD} = 0.5 mm) with scan rate, v, in a range of 0.05 to 1.0 V s^{-1}.

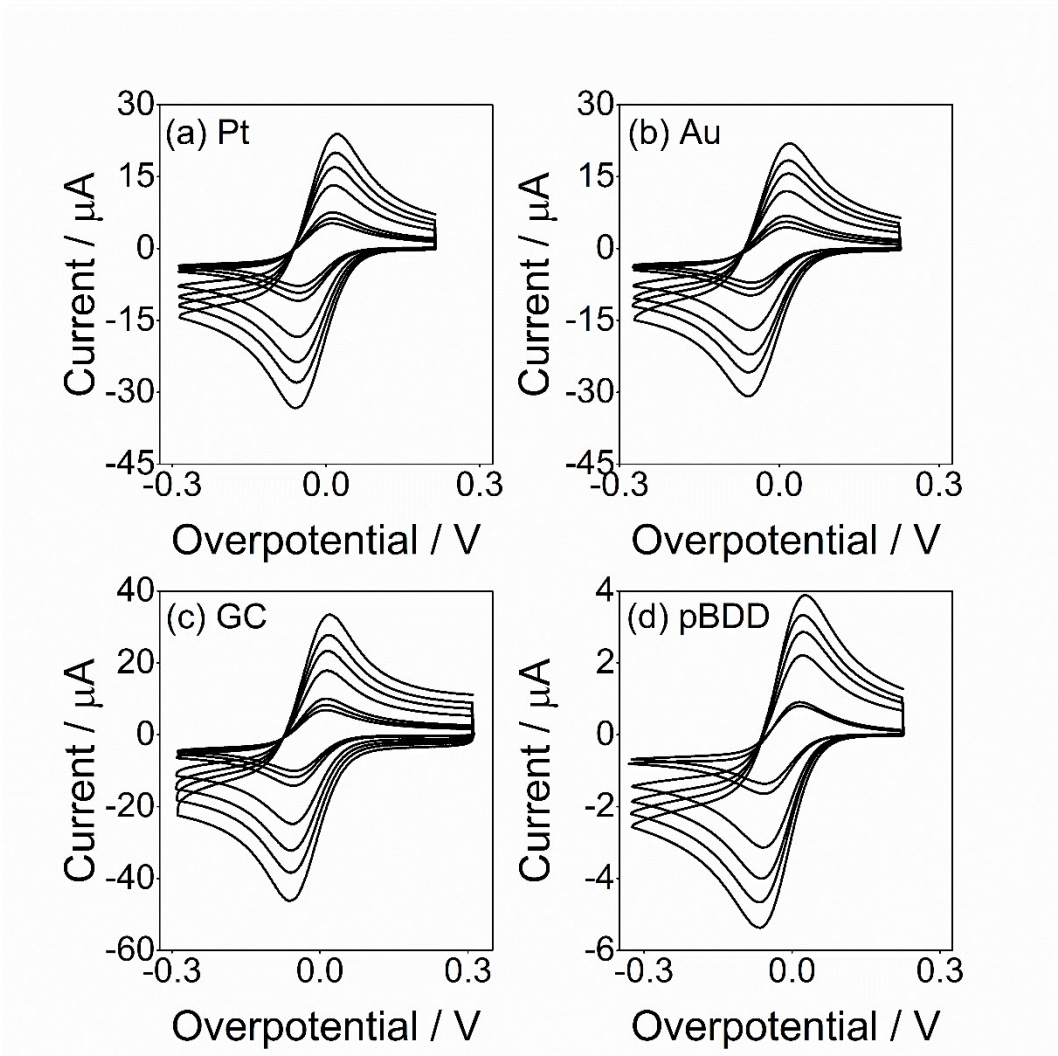

Figure S2. CVs for the reduction of 1.0 mM TCNQ in CH_3CN (0.1 M Bu_4NPF_6) at (a) Pt (a_{Pt} = 1.0 mm), (b) Au (a_{Au} = 1.0 mm), (c) GC (a_{GC} = 1.5 mm) and (d) pBDD (a_{pBDD} = 0.5 mm) with v in a range of 0.05 to 1.0 V s^{-1}.

Section S5: Determination of the diffusion coefficients of TTF and TCNQ

CVs for the oxidation of 1.0 mM TTF and reduction of 1.0 mM TCNQ taken at a Pt UME (a = 1.0 μm) are shown in Figure S-4a and b, respectively. The measured diffusion-limited current, i_{UME}, gave diffusion coefficients, $D_{TTF} = 2.10 \times 10^{-5}$ cm^2 s^{-1} and $D_{TCNQ} = 1.66 \times 10^{-5}$ cm^2 s^{-1}.

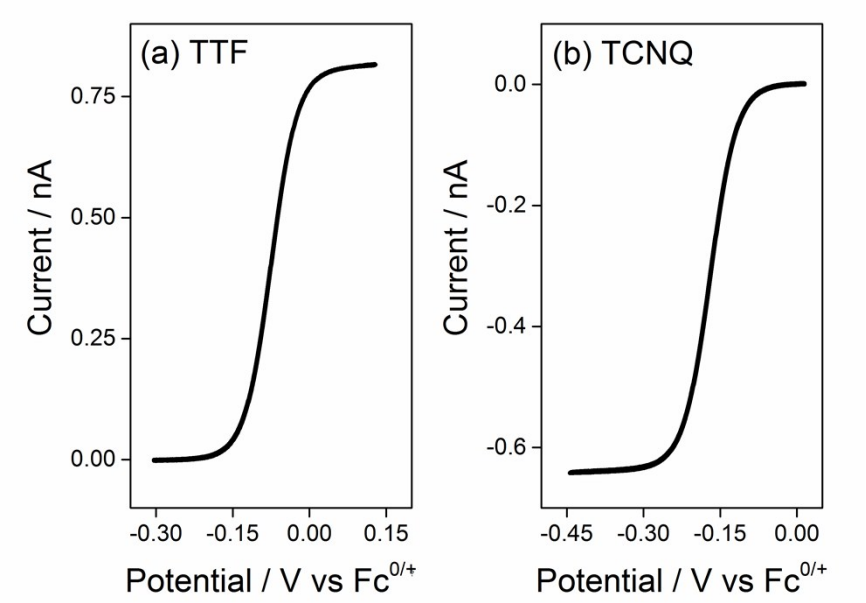

Figure S3. CVs for the (a) oxidation of 1.0 mM TTF and (b) reduction of 1.0 mM TCNQ in CH_3CN (0.1 M Bu_4NPF_6) with v = 0.05 V s^{-1} at a 1.0 μm-radius Pt UME.

Section S6: Determination of the diffusion coefficients of $TTF^{\bullet+}$ and $TCNQ^{\bullet-}$

Voltammetric studies in the SECM configuration are very sensitive to differences in *D* values of the oxidized and reduced forms of the redox couple. It is rare for the diffusivities of both redox forms to be the same, particularly in organic (non-conventional) solvents, studied herein. Accurate determination of these values are very important for accurate quantitative kinetic studies,[10–14] especially if one is seeking to measure the kinetics of fast processes that are close to the diffusion-limit.

To accurately determine *D* of $TTF^{\bullet+}$ and $TCNQ^{\bullet-}$, we employed SECM-chronoamperometric measurements with a Pt UME in both feedback[11] and SG/TC modes.[13] The UME tip responses can be analyzed to give the *D* ratio of the oxidized to reduced form of the redox couple, γ, when the redox couple undergoes a simple diffusion-controlled one ET, with no kinetic complications and adsorption effects.[11,13,15] In the feedback configuration, γ has no effect on the steady-state current measured at the UME tip[11] because the feedback steady-state limiting-current merely depends on the redox competition between the substrate and tip electrodes in the solution. Hence, the feedback mode limiting-current can be used to precisely determine the tip-substrate separation for a pair of feedback and SG/TC limiting-currents taken at the same tip position. Under the SG/TC SECM-chronoamperometric configuration, $TTF^{\bullet+}$ or $TCNQ^{\bullet-}$ is electrogenerated at a diffusion-controlled rate from the precursor in bulk (TTF or TCNQ), at a macroscopic Pt substrate. The $TTF^{\bullet+}$ or $TCNQ^{\bullet-}$ diffusion front is intercepted by the UME tip positioned close to the substrate. Although the macroscopic substrate electrode will have a transient form, the redox mediator diffusional cycling between the UME tip and substrate will be in a quasi-steady-state limited by the diffusion of $TTF^{\bullet+}$ or $TCNQ^{\bullet-}$. Therefore, the limiting-current measured in the SG/TC mode can be used to determine γ from a simple modification of an empirically derived equation for the positive feedback mode:[16]

$$I_{\mathrm{UME,lim}}(L) = \gamma\left[0.68 + 0.78377/L + 0.3315\exp(-1.0672L)\right] \qquad \text{(eqn S12)}$$

Section S7: FTACV experimental and simulated data for the oxidation of TTF at Au and GC macroelectrodes

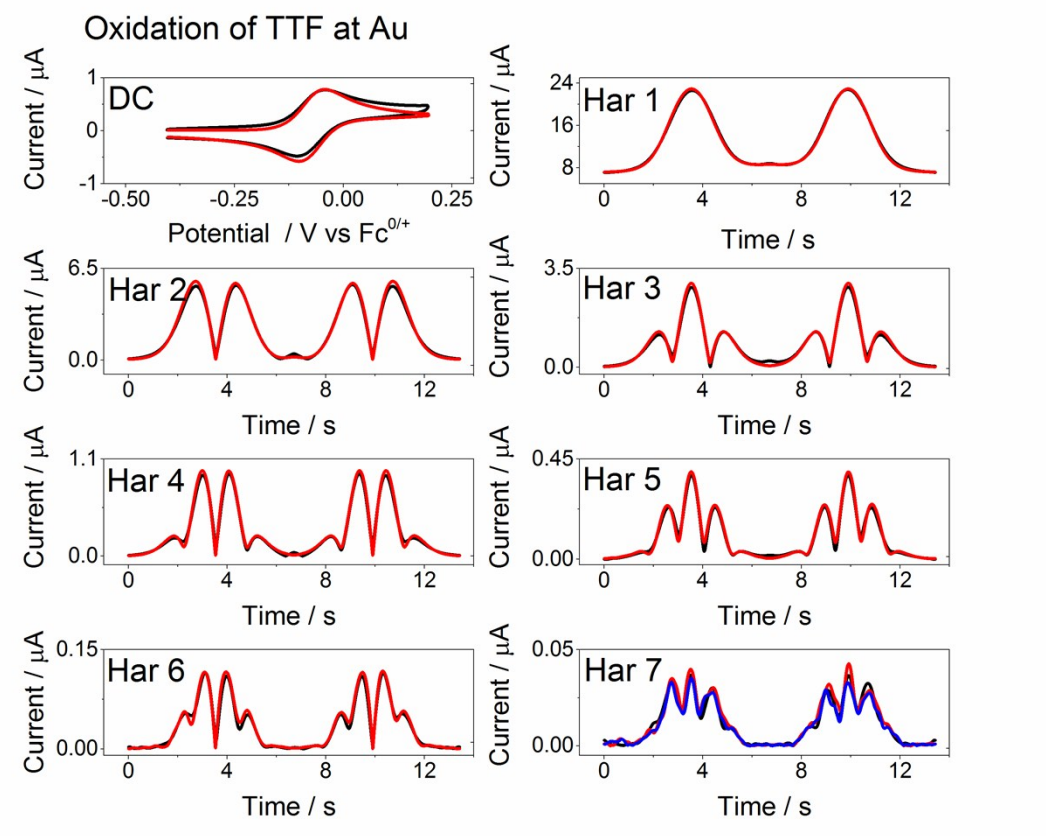

Figure S4. Comparison of experimental (black lines) and simulated (red lines, $\Psi = 0.994$) FTACV curves for the one-electron oxidation of 0.25 mM TTF in CH_3CN (0.1 M Bu_4NPF_6) at an Au macroelectrode. Simulation parameters: $k^0 = 1000$ cm s^{-1} (reversible), $\alpha = 0.50$, $R_u = 500$ ohm, $A = 0.00785$ cm^2, $f = 228.0$ Hz, $\Delta E = 80.0$ mV, $D_{TTF} = 2.10 \times 10^{-5}$ cm^2 s^{-1}, $D_{TTF^{\bullet+}} = 1.80 \times 10^{-5}$ cm^2 s^{-1}, $v_{AC} = 0.07$ V s^{-1} and $v_{DC} = 0.1$ V s^{-1}. The blue line shows the 7th AC harmonic component response for $k^0 = 1.5$ cm s^{-1} with all other simulation parameters the same and represents the upper kinetic limit of detection.

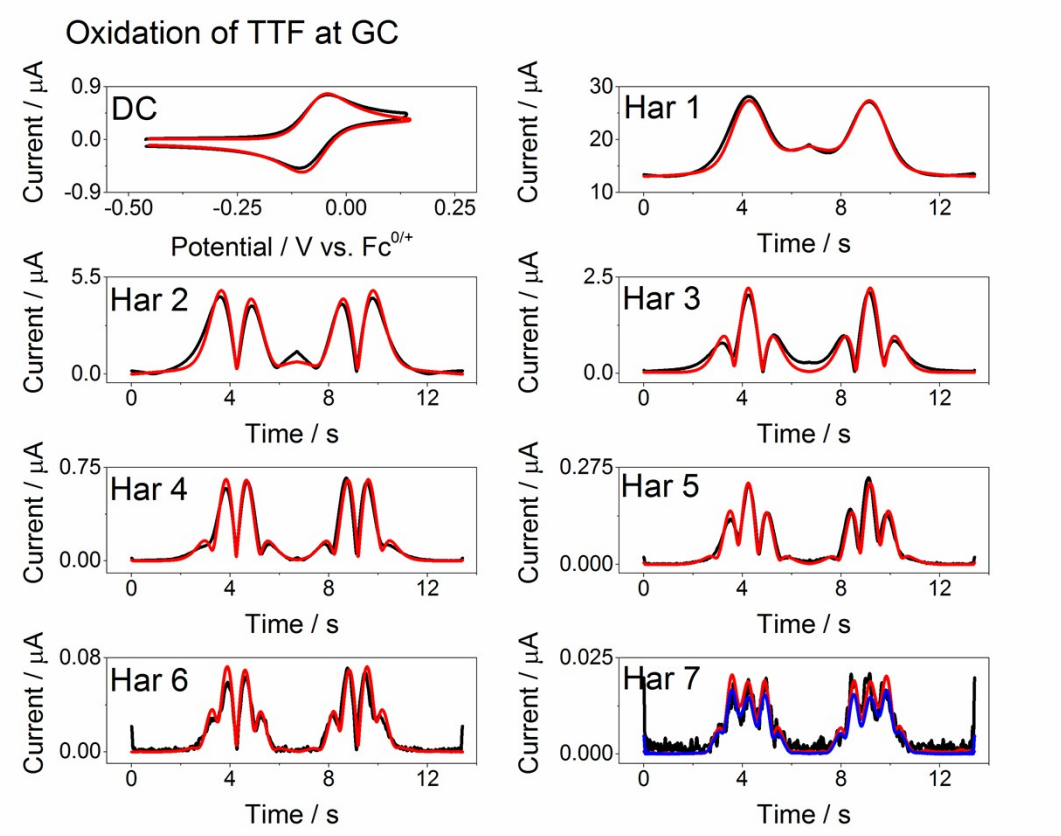

Figure S5. Comparison of experimental (black lines) and simulated (red lines, $\Psi = 0.975$) FTACV curves for the one-electron oxidation of 0.25 mM TTF in CH_3CN (0.1 M Bu_4NPF_6) at a GC macroelectrode. Simulation parameters: $k^0 = 1000$ cm s^{-1} (reversible), $\alpha = 0.50$, $R_u = 525$ ohm, $A = 0.00785$ cm^2, $f = 228.0$ Hz, $\Delta E = 80.0$ mV, $D_{TTF} = 2.10 \times 10^{-5}$ cm^2 s^{-1}, $D_{TTF^{\bullet+}} = 1.80 \times 10^{-5}$ cm^2 s^{-1}, $v_{AC} = 0.09$ V s^{-1} and $v_{DC} = 0.1$ V s^{-1}. The blue line shows the 7th AC harmonic component response for $k^0 = 1.0$ cm s^{-1} with all other simulation parameters the same and represents the upper kinetic limit of detection.

Section S8: FTACV experimental and simulated data for reduction of TCNQ at Pt, Au, GC and pBDD macroelectrodes

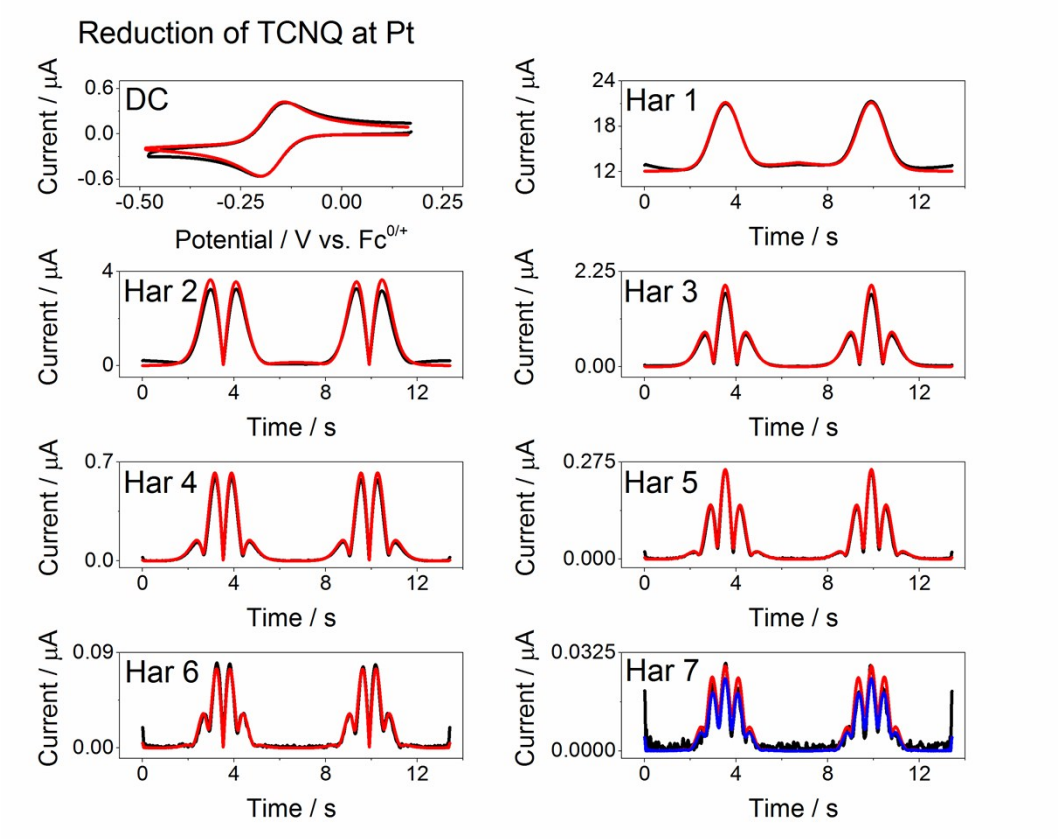

Figure S6. Comparison of experimental (black lines) and simulated (red lines, $\Psi = 0.990$) FTACV curves for the one-electron oxidation of 0.20 mM TCNQ in CH_3CN (0.1 M Bu_4NPF_6) at a Pt macroelectrode. Simulation parameters: $k^0 = 1000$ cm s^{-1} (reversible), $\alpha = 0.50$, $R_u = 550$ ohm, $A = 0.00785$ cm^2, $f = 228.0$ Hz, $\Delta E = 80.0$ mV, $D_{TCNQ} = 1.66 \times 10^{-5}$ cm^2 s^{-1}, $D_{TCNQ^{\bullet-}} = 1.53 \times 10^{-5}$ cm^2 s^{-1} and $v_{AC} = v_{DC} = 0.1$ V s^{-1}. The blue line shows the 7th AC harmonic component response for $k^0 = 1.2$ cm s^{-1} with all other simulation parameters the same and represents the upper kinetic limit of detection.

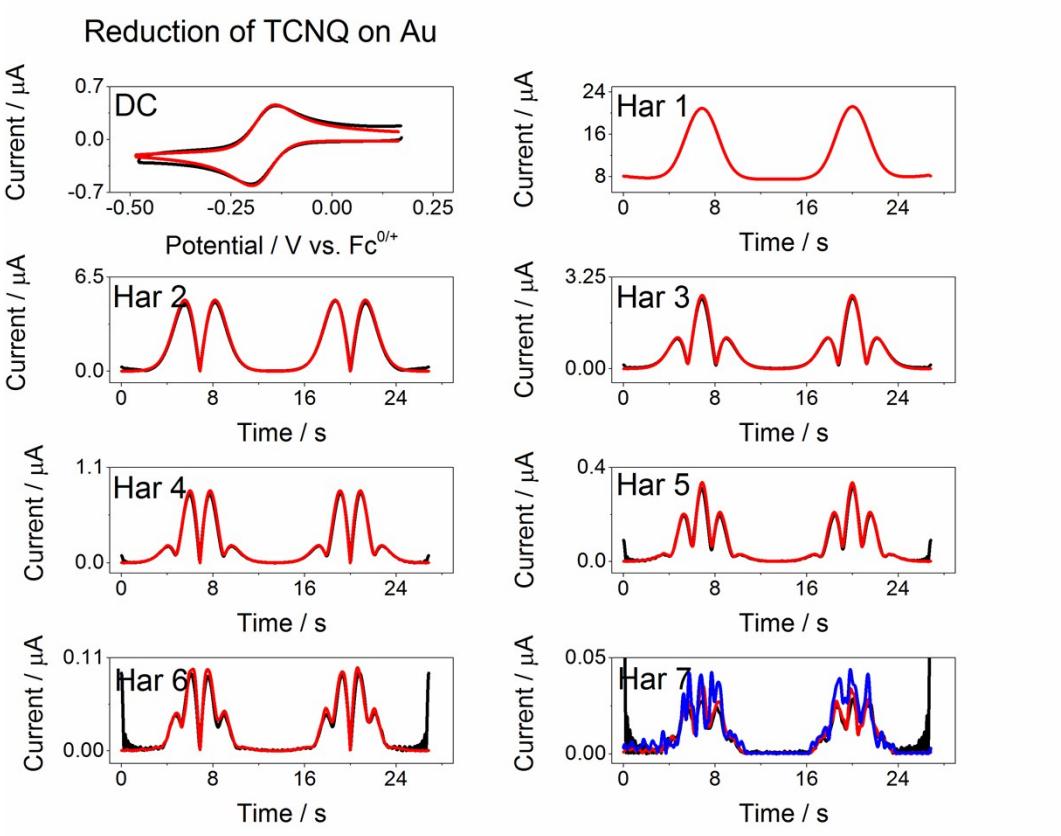

Figure S7. Comparison of experimental (black lines) and simulated (red lines, $\Psi = 0.990$) FTACV curves for the one-electron oxidation of 0.20 mM TCNQ in CH_3CN (0.1 M Bu_4NPF_6) at an Au macroelectrode. Simulation parameters: $k^0 = 1.0$ cm s^{-1}, $\alpha = 0.50$, $R_u = 485$ ohm, $A = 0.00785$ cm^2, $f = 228.0$ Hz, $\Delta E = 80.0$ mV, $D_{TCNQ} = 1.66 \times 10^{-5}$ cm^2 s^{-1}, $D_{TCNQ^{\bullet-}} = 1.53 \times 10^{-5}$ cm^2 s^{-1}, $v_{AC} = 0.05$ V s^{-1} and $v_{DC} = 0.1$ V s^{-1}. The blue line shows the 7th AC harmonic component response for a reversible process ($k^0 = 1000$ cm s^{-1}) with all other simulation parameters the same.

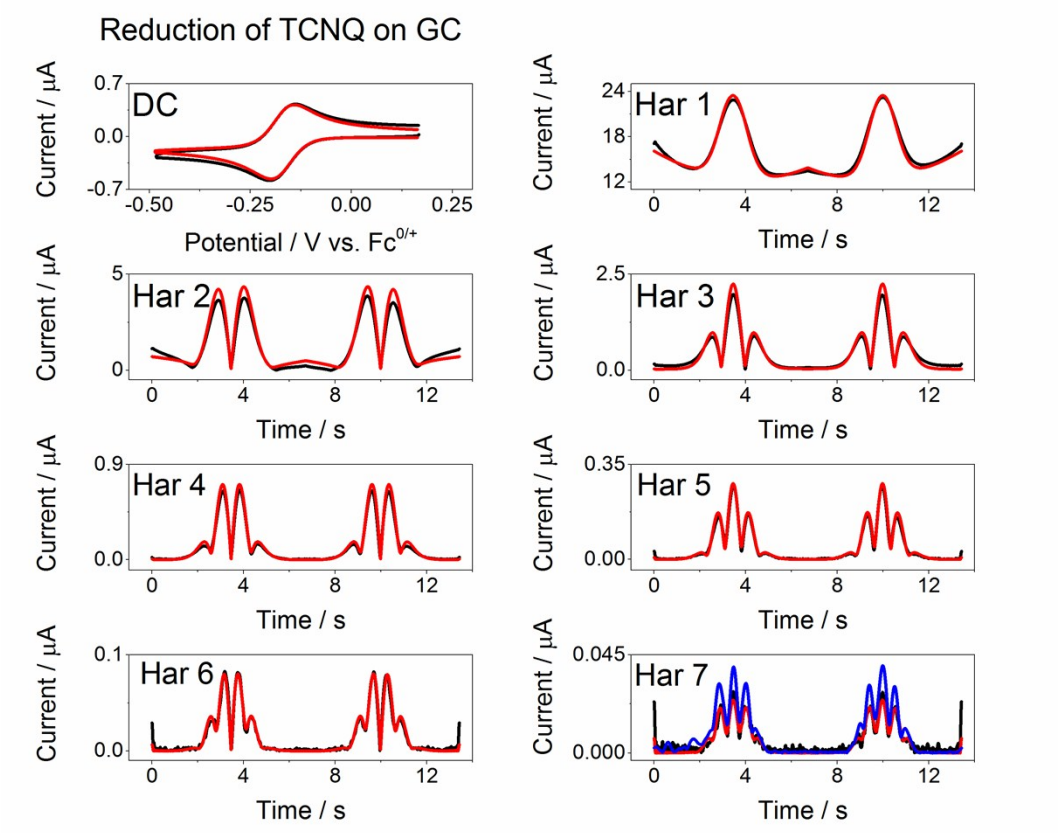

Figure S8. Comparison of experimental (black lines) and simulated (red lines, $\Psi = 0.981$) FTACV curves for the one-electron oxidation of 0.20 mM TCNQ in CH_3CN (0.1 M Bu_4NPF_6) at a GC macroelectrode. Simulation parameters: $k^0 = 1.0$ cm s^{-1}, $\alpha = 0.50$, $R_u = 475$ ohm, $A = 0.00785$ cm^2, $f = 228.0$ Hz, $\Delta E = 80.0$ mV, $D_{TCNQ} = 1.66 \times 10^{-5}$ cm^2 s^{-1}, $D_{TCNQ^{\bullet-}} = 1.53 \times 10^{-5}$ cm^2 s^{-1} and $v_{AC} = v_{DC} = 0.1$ V s^{-1}. The blue line shows the 7th AC harmonic component response for a reversible process ($k^0 = 1000$ cm s^{-1}) with all other simulation parameters the same.

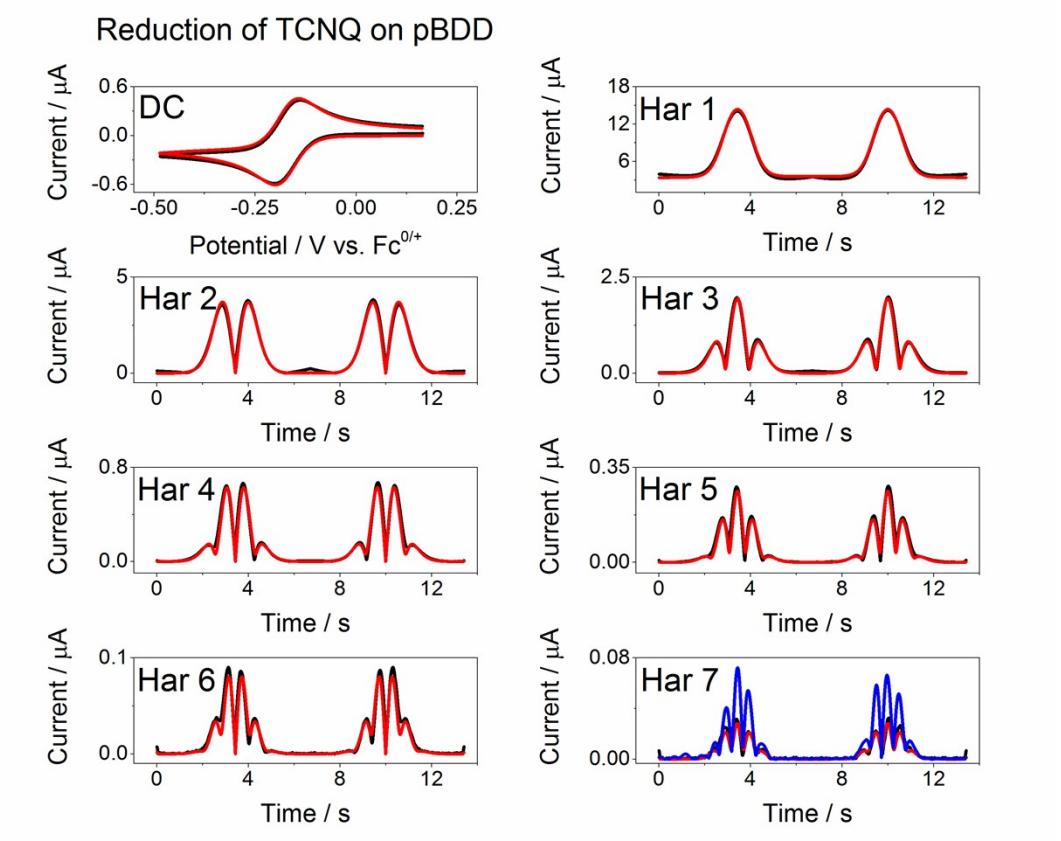

Figure S9. Comparison of experimental (black lines) and simulated (red lines, $\Psi = 0.979$) FTACV curves for the one-electron oxidation of 0.20 mM TCNQ in CH_3CN (0.1 M Bu_4NPF_6) at a pBDD macroelectrode. Simulation parameters: $k^0 = 0.4$ cm s^{-1}, $\alpha = 0.50$, $R_u = 300$ ohm, $A = 0.00785$ cm^2, $f = 228.0$ Hz, $\Delta E = 80.0$ mV, $D_{TCNQ} = 1.66 \times 10^{-5}$ cm^2 s^{-1}, $D_{TCNQ^{\bullet-}} = 1.53 \times 10^{-5}$ cm^2 s^{-1} and $v_{AC} = v_{DC} = 0.1$ V s^{-1}. The blue line shows the 7th AC harmonic component response for a reversible process ($k^0 = 1000$ cm s^{-1}) with all other simulation parameters the same.

References

1 A. A. Sher, A. M. Bond, D. J. Gavaghan, K. Harriman, S. W. Feldberg, N. W. Duffy, S.-X. Guo and J. Zhang, *Anal. Chem.*, 2004, **76**, 6214–6228.

2 A. M. Bond, N. W. Duffy, D. M. Elton and B. D. Fleming, *Anal. Chem.*, 2009, **81**, 8801–8808.

3 A. J. Bard and L. R. Faulkner, *Electrochemical Methods: Fundamentals and Applications*, Wiley, New York, 2nd edn., 2001.

4 C. M. A. Brett and A. M. O. Brett, *Electrochemistry: Principles , Methods , and Applications*, 1994.

5 G. P. Morris, A. N. Simonov, E. A. Mashkina, R. Bordas, K. Gillow, R. E. Baker, D. J. Gavaghan and A. M. Bond, *Anal. Chem.*, 2013, **85**, 11780–11787.

6 A. N. Simonov, G. P. Morris, E. A. Mashkina, B. Bethwaite, K. Gillow, R. E. Baker, D. J. Gavaghan and A. M. Bond, *Anal. Chem.*, 2014, **86**, 8408–8417.

7 E. A. Mashkina, A. N. Simonov and A. M. Bond, *J. Electroanal. Chem.*, 2014, **732**, 86–92.

8 K. McKelvey, M. A. Edwards and P. R. Unwin, *Anal. Chem.*, 2010, **82**, 6334–6337.

9 C. Lefrou, *J. Electroanal. Chem.*, 2006, **592**, 103–112.

10 N. Nioradze, J. Kim and S. Amemiya, *Anal. Chem.*, 2011, **83**, 828–835.

11 R. D. Martin and P. R. Unwin, *J. Electroanal. Chem.*, 1997, **439**, 123–136.

12 J. Ghilane, C. Lagrost and P. Hapiot, *Anal. Chem.*, 2007, **79**, 7383–91.

13 R. D. Martin and P. R. Unwin, *Anal. Chem.*, 1998, **70**, 276–284.

14 D. Mampallil, K. Mathwig, S. Kang and S. G. Lemay, *Anal. Chem.*, 2013, **85**, 6053–6058.

15 S.-y. Tan, J. Zhang, A. M. Bond, J. V. Macpherson and P. R. Unwin, *Anal. Chem.*, 2016, **88**, 3272–3280.

16 M. V. Mirkin, F.-R. F. Fan and A. J. Bard, *J. Electroanal. Chem.*, 1992, **328**, 47–62.